

Probabilistic Modeling of Blood Vessels for Segmenting Magnetic Resonance Angiography Images

Probabilistic Modeling of Blood Vessels for Segmenting Magnetic Resonance Angiography Images

Authors & Affiliations

Ahmed Shalaby

*BioImaging Lab, University of
Louisville, KY, USA*

Fatma Taher

*Department of Electrical and
Computer Engineering, Khalifa
University, Abu Dhabi, UAE*

Maryam El-Baz

*BioImaging Lab, University of
Louisville, KY, USA*

Mohammed Ghazal

*Electrical and Computer
Engineering Department Abu
Dhabi University, Abu Dhabi, UAE*

Mohamed Abou El-Ghar

*Radiology Department, Urology
and Nephrology Center, University
of Mansoura, Egypt.*

Ali Takieldean

*BioImaging Lab, University of
Louisville, KY, USA*

Correspondence

Ayman El-Baz

*BioImaging Lab, University of
Louisville, KY, USA*

ayman_elbazz@yahoo.com

Abstract

A new adaptive probabilistic model of blood vessels on magnetic resonance angiography (MRA) images is proposed. The model accounts for both laminar (for normal subjects) and turbulent blood flows (in abnormal cases like anemia or stenosis) and results in a fast algorithm for extracting a 3D cerebrovascular system from MRA data. To accurately separate blood vessels from other regions of interest, the marginal distribution is precisely approximated with an adaptive linear combination of the derived model and a number of dominant and subordinate discrete Gaussians, rather than with a mixture of only three pre-selected Gaussian and uniform or Rician components. To validate the accuracy of the proposed algorithm, a special 3D geometrical phantom motivated by statistical analysis of the time-of-flight MRA (TOF-MRA) data is designed. Experiments with synthetic and 50 real data sets confirm the high accuracy and reduced computational cost of the proposed approach.

Keywords: MRA, PC-MRA, TOF-MRA, Vascular Signal

Probabilistic Modeling of Blood Vessels for Segmenting Magnetic Resonance Angiography Images

1. Introduction

Accurate 3D cerebrovascular system segmentation from magnetic resonance angiography (MRA) images is one of the most important problems in practical computer-assisted medical diagnostics. Phase Contrast MRA (PC-MRA) provides good suppression of background signals and quantifies blood flow velocity vectors for each voxel. time-of-flight MRA (TOF-MRA) is less quantitative, but it is fast and produces images with high contrast. The most popular techniques for extracting blood vessels from MRA data are scale-space filtering, centerline based methods, deformable models, statistical models, and hybrid methods.

Multiscale filtering enhances curvilinear structures in 3D medical images by convolving an image with Gaussian filters at multiple scales [4-7]. Eigenvalues of the Hessian at each voxel are analyzed to determine the local shapes of 3D structures (by the eigenvalues, voxels from a linear structure, like a blood vessel, differ from those for a planar structure, speckle noise, or unstructured components). The multiscale filter output forms a new enhanced image

such that the curvilinear structures become brighter whereas other components become darker [4]. Such an image can be directly visualized, thresholded, and segmented using a deformable model. Alternatively, the obtained eigenvalues define a candidate set of voxels corresponding to the centerlines of the vessels [5]. Multiscale filter responses at each of the candidates determine the likelihood that a voxel belongs to a vessel of each particular diameter. The maximal response over all the diameters (scales) is assigned to each voxel, and a surface model of the entire vascular structure is reconstructed from the estimated centerlines and diameters. After segmenting the filtered MRA image using thresholding, anisotropic diffusion techniques are used to remove noise, while preserving small vessels [6]. Lacoste et al. [7] proposed a multiscale technique based on Markov marked point processes to extract coronary arteries from 2D X-ray angiograms. Coronary vessels are modeled locally as piece-wise linear segments of varying locations, lengths, widths and orientations. The vessels' centerlines are extracted using a Markov object process modeled by a uniform Poisson process. Process optimization

Probabilistic Modeling of Blood Vessels for Segmenting Magnetic Resonance Angiography Images

was achieved via simulated annealing using a reversible Markov chain Monte Carlo algorithm.

Centerline minimal path-based techniques [8-10] formulate the two-point centerline extraction as the minimum cost integrated along the centerline path. Gu'lsu'n and Tek [8] used multi-scale medialness filters to compute the cost of graph edges in a graph-based minimal path detection method to extract the vessels' centerlines. A post processing step, based on the length and scale of vessel centerlines, was performed to extract the full vessel centerline tree. P'echaud et al. [9] presented an automatic framework to extract tubular structures from 2D images by the use of shortest paths. Their framework combined multiscale and orientation optimization to propagate 4D (space + scale + orientation) paths on the 2D images. Li and Yezzi [10] represented the 3D vessel surface as a

4D curve, with an additional non-spatial dimension that described the radius (thickness) of the vessel. They applied a minimal path approach to find the minimum path between user defined end points in the 4D space. The detected path simultaneously described the

vessel centerline as well as its surface. To overcome the possible shortcut problem of minimal path techniques (i.e., track a false straight shortcut path instead of following the true curved path of the vessel), Zhu and Chung [11] used a minimum average-cost path model to segment the 3D coronary arteries from CT images. In their approach, the average edge cost is minimized along paths in the discrete 4D graph constructed by image voxels and associated radii.

Deformable model approaches to 3D vascular segmentation attempt to approximate the boundary surface of the blood vessels [12-17]. An initial boundary, called a snake [18], evolves in order to optimize a surface energy which depends on image gradients and surface smoothness. To increase the capture range of the evolving boundary, Xu and Prince [19] used a gradient vector flow (GVF) field as an additional force to drive snakes into object concavities, which was later used to segment the blood vessels from 3D MRA [12]. Geodesic active contours [20] implemented with level set techniques offer flexible topological adaptability to segment the MRA images [13] including more efficient adaptation to local geometric

Probabilistic Modeling of Blood Vessels for Segmenting Magnetic Resonance Angiography Images

structures represented. Fast segmentation of blood vessel surfaces is obtained by inflating a 3D balloon with fast marching methods [14].

Holtzman-Gazit et al. [15] extracted blood vessels in Computed tomography angiography (CTA) images based on variational principles. Their framework combined the Chan-Vese minimal variance model with a geometric edge alignment measure and the geodesic active surface model. Manniesing et al. [16] proposed a level set-based vascular segmentation method for finding vessel boundaries in CTA images. The level set function is attracted to the vessel boundaries based on a dual object (vessels) and background intensity distributions, which are estimated from the intensity histogram. Recently, Forkert et al. [17] used a vesselness filter to guide the direction of a level set to extract vessels from TOF-MRA data. Compared to scale-space filtering, deformable models produce much better experimental results, but have a common drawback, namely, manual initialization. Also, both group approaches are slow when compared to statistical approaches.

Statistical extraction of a vascular tree is completely

automatic, but its accuracy depends on the underlying probability models. The MRA images are multi-modal in that the signals (intensities, or gray levels) in each region of interest (e.g., blood vessels, brain tissues, etc) are associated with a particular dominant mode of the total marginal probability distribution of signals. To the best of our knowledge, adaptive statistical approaches for extracting blood vessels from the MRA images have been proposed so far only by Wilson and Noble [21] for the TOF-MRA data and Chung and Noble [22] for the PC-MRA data. The former approach represents the marginal data distribution with a mixture of two Gaussians and one uniform component for the stationary cerebrospinal fluid (CSF), brain tissues, and arteries, respectively, whereas the latter approach replaces the Gaussians with the more adequate Rician distribution. To identify the mixture (i.e., estimate all its parameters) a conventional EM algorithm is used in both cases. It was called a "modified EM" in [21], after replacing gray levels in individual pixels considered by their initial EM scheme with a marginal gray level distribution. Actually, such a modification returns to what has been in common use for

Probabilistic Modeling of Blood Vessels for Segmenting Magnetic Resonance Angiography Images

decades for density estimation (see e.g., [23]), while the individual pixels appeared in their initial scheme only as a verbatim replica of a general EM framework.

Different hybrid approaches have attempted to combine the aforementioned approaches. For instance, a region-based deformable contour for segmenting tubular structures is derived in [24] by combining signal statistics and shape information. Law and Chung [25] guided a deformable surface model with the second order intensity statistics and surface geometry to segment blood vessels from TOF- and PC-MRA images. A combination of a Gaussian statistical model with the maximum intensity projection images acquired at three orthogonal directions [26] allows for extracting blood vessels iteratively from images acquired by rotational angiography. Alternatively, Hu et al. [27] extracted the object boundaries by combining an iterative thresholding approach with region growing and component label analysis.

Mille et al. [28] used a generalized cylinder (GC) region-based deformable model for the segmentation of the angiogram. The GC is modeled as a central planar curve, acting

as a medial axis, and variable thickness. The GC is deformed by coupling the evolution of the curve and thickness using narrow band energy minimization. This energy was transformed and derived in order to allow implementation on a polygonal line deformed using a gradient descent approach. Tyrrell et al. [29] proposed a super-ellipsoid geometric model to extract the vessel boundaries from in-vivo optical slice data. Their approach predicted the direction of the centerline utilizing a statistical estimator. Chen and Metaxas [30] combined a prior Gibbs random field model, marching cubes, and deformable models. First, the Gibbs model is used to estimate object boundaries using region information from 2D slices. Then, the estimated boundaries and the marching cubes technique are used to construct a 3D mesh specifying the initial geometry of a deformable model. Finally, the deformable model fits the data under the 3D image gradient forces.

Recently, Shang et al. [31] developed an active contour framework to segment coronary artery and lung vessel trees from CT images. A region, competition based active contour model is used to segment thick vessels based on

Probabilistic Modeling of Blood Vessels for Segmenting Magnetic Resonance Angiography Images

a Gaussian mixture model of the gray-level distribution of the vessel region. Then, a multiscale vector field, derived from the Hessian matrix of the image intensity, is used to guide the active contour through thin vessels. Finally, the surface of the vessel is smoothed using a "vesselness" function that selects between a minimal principal curvature and a mean curvature criterion. Gao et al. [32] used a statistical model to find the main cerebrovascular structure from TOF-MRA. Then, an edge-strength function that incorporates statistical region distribution and gradient information is used to guide a 3D geometric deformable model to deal with the under-segmentation problem. Dufour et al. [33] proposed an interactive segmentation method that incorporates component-trees and example based segmentation to extract the cerebrovascular tree from TOF-MRA data. Liao et al. [34] used a parametric intensity model to extract thick and most thin vessels from 7 Tesla MRA images. To fill the remaining gaps, a generative Markov random field method was applied.

The previous overview shows the following limitations of the existing approaches:

1. Most of them presume only a single image type (e.g., TOF- or PC-MRA).
2. Most of them require user interaction to initialize a vessel of interest.
3. Some deformable models assume circular vessel cross sections; this holds for healthy people, but not for patients with a stenosis or an aneurysm.
4. All but statistical approaches are computationally expensive.
5. Known statistical approaches use only predefined probability models that cannot fit all the cases because actual intensity distributions for blood vessels depend on the patient, scanner, and scanning parameters.

The rest of the paper is organized as follows: in Section 2, we briefly discuss the proposed probability model of vascular signals and the adaptive model of Multi-modal MRA. Section 3 presents the experiments of proposed segmentation methodology of the blood vessels. Section 4 explains the validation, and compares our results with other alternatives. Finally,

Probabilistic Modeling of Blood Vessels for Segmenting Magnetic Resonance Angiography Images

conclusions are drawn in Section 5.

2. The Proposed Method

This paper derives a more general probabilistic model of blood vessels on MRA images to account for normal and abnormal states of the vascular system, i.e. for both laminar and turbulent blood flow without and with stenosis. To accurately separate blood vessels from other regions-of-interest, the marginal distribution is precisely approximated with an adaptive linear combination of the derived model and a number of dominant and subordinate discrete Gaussians rather than with a mixture of only three pre-selected Gaussian and uniform or Rician components. Experiments show that our adaptive model results in significantly improved segmentation of MRA images. More physical and mathematical foundation of the proposed method can be found in [36-42].

2.1. Probability Model of Vascular Signals

Conventional models of intensities for vessel voxels in [1, 21] assume laminar blood flow with parabolic velocity flow through a circular cross-section of the vessel [2]. Let $q; q \in \mathbf{Q} = \{0, 1, \dots, Q-1\}$, be the Q -

ary signals (image intensity, or gray level). Then the intensity profile for a vessel is $q_r = q_{\max} \left(1 - \frac{r^2}{R^2}\right)$ where q_r is the intensity at the distance r from the center of a vessel of radius R and the constant $q_{\max} \leq Q - 1$ depends on the scanner. In this case the intensities over the circular cross-section are distributed uniformly with the probability

density: $\varphi_{\text{lam}}(q) = \frac{1}{q_{\max}}$ in the range $[0, q_{\max}]$. Nonetheless, the laminar flow holds only for subjects with normal vascular systems [3].

Various diseases change either blood velocity or viscosity or both and cause the turbulent flow. Turbulence depends on the diameter of vessel and blood velocity and viscosity. For example, due to lower blood viscosity, anemia leads frequently to turbulence. Artery constrictions increasing blood velocity (see Fig. 1) and vascular diseases such as thrombosis, embolism, thyrotoxicosis, atherosclerosis, and valvular heart diseases also result in turbulence [3].

Since the MRA may represent both normal and abnormal subjects, the model of vascular signals can be built as a mixture of the laminar and turbulent components [38, 39]:

Probabilistic Modeling of Blood Vessels for Segmenting Magnetic Resonance Angiography Images

$$\varphi(q) = (1 - \beta)\varphi_{lam}(q) + \beta\varphi_{turb}(q) \equiv \frac{1 - 2\beta}{q_{max}} + \frac{\beta}{\sqrt{q_{max}(q_{max} - q)}} \quad (1)$$

Probability densities for different mixing weights $\beta \in [0,1]$ in this model are presented in Fig. 2.

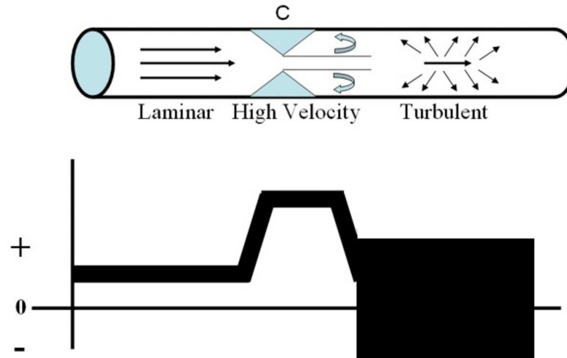


Figure 1: Influence of constriction (C) on the blood velocities in a vessel (arrows indicate flow directions) and ranges of velocities at each cross-section along the vessel [3].

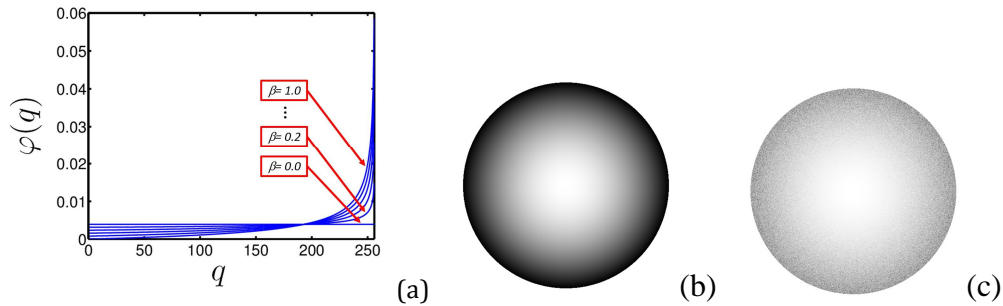


Figure 2: Probability densities for Eq. (1) with $\beta = 0.0, 0.2, 0.4, \dots, 1.0$ and synthetic crosssection images of a blood vessel with laminar ($\beta = 0$, b) and turbulent ($\beta = 1$, c) flow.

2.2. Adaptive Model of Multi-modal MRA

MRA images contain three regions-of-interest (signal classes): (i) darker CSF from bones and fat, (ii) brain tissues

(gray matter and white matter), and (iii) brighter blood vessels. Marginal signal distributions for the first two classes are typically of intricate shape that differs much from the conventional individual Gaussians in [1, 21].

Probabilistic Modeling of Blood Vessels for Segmenting Magnetic Resonance Angiography Images

The model in Eq.(1) describes only circular vessels and should have additional terms changing its shape to account for variations of the blood flow due to stenosis. Generally, no predefined probability model can accurately describe all the signal variations due to changes in blood velocity and viscosity, vessel diameter, and scanner sensitivity.

$$PMRA(q) = \sum_{i \in (bv, csf, br)} \alpha_i \varphi_i(q) \quad (2)$$

where α_i are the mixing weights ($\alpha_1 + \alpha_2 + \alpha_3 = 1$). Each of the three submodels $\varphi_i(q)$ is a mixture of one dominant component with a linear combination of several sign-alternate subordinate components chosen to closely approximate corresponding parts of an empirical marginal signal distribution

$$F_{emp} = (f_{emp}(q) : q \in \mathbf{Q}).$$

The subordinate part of each submodel $\varphi_i(q)$ is a linear combination of discrete Gaussians (LCDGs) with $C_{i,p}$

$$G(\beta) = \sum_{q=0}^{q_{max}} \pi(i = bv | q) f_{emp}(q) \ln \varphi_{bv}(q | \beta) \quad (3)$$

where $\pi(i | q)$ is the responsibility of the submodel i for q [36, 41].

3. Segmentation of blood vessels

To justify the adaptive model of Eq. (2), Fig. 3 shows how

Therefore, we propose an adaptive probability model to handle both normal and abnormal MRA images. It mixes three submodels representing the above-mentioned major image areas (abbreviated by “csf”, “br”, and “bv”, respectively) [37, 41]:

positive and $C_{i,n}$ negative components under obvious restrictions on their weights [42-45]. To identify the three submodels (estimate parameters of their dominant components and numbers and parameters of the positive and negative subordinate components), we use the EM-based techniques introduced in [35]. The only difference here is in the nonanalytical estimation of the parameter β on the M-steps using the gradient-based search for the global maximum of the goal likelihood function:

different scanners effect the measurements. These three TOF-MRA slices were acquired for a subject with anemia using

Probabilistic Modeling of Blood Vessels for Segmenting Magnetic Resonance Angiography Images

a Picker 1.5T Edge MRI scanner with resolution of $512 \times 512 \times 93$, a subject with parietal lobe hemorrhage using a Signa Horizon GE 1.5T scanner with resolution $512 \times 512 \times 150$, and

a normal subject using a state-of-art Siemens 3T scanner with resolution $512 \times 512 \times 125$, respectively. The slice thickness is 1 mm in all the cases.

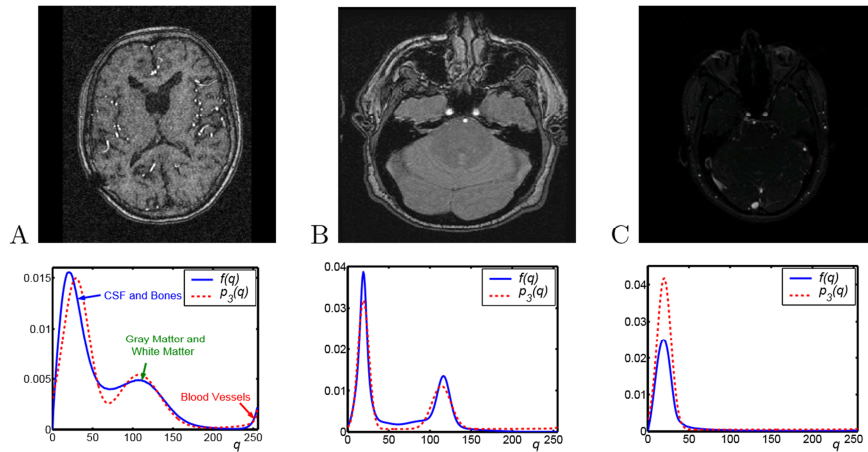


Figure 3: Three TOF-MRA slices with their empirical distributions $f_{\text{emp}}(q)$ overlaid with the dominant mixtures $p_3(q)$.

The models of Eq. (2) were built with the EM-based approach (see [35] for detail). Figure 3 presents both the marginal empirical distributions F_{emp} and the initial 3-component dominant mixtures for them containing the two Gaussian components and our model of blood vessels in Eq. (1). The estimated parameters β of the latter are 0.92, 0.18, and 0.038 for the slices A, B, and C in Fig. 3, respectively, that reflects levels of blood turbulence expected from physics-based considerations.

Figure 4 illustrates basic stages of our EM-based initialization and final refinement of the whole model of Eq. (2) for the slice A. Given the dominant mixture $P_3 = (p_3(q) : q \in \mathbf{Q})$, the number and the parameters of the subordinate DGs are estimated from the absolute deviations $f_{\text{emp}}(q) - p_3(q)$ by minimizing the residual approximation error. In this case the eight DGs are added to the dominant mixture to obtain the best initial 3-class model. The final model is obtained using the EM-based

Probabilistic Modeling of Blood Vessels for Segmenting Magnetic Resonance Angiography Images

refinement (here, the first nine refining iterations increase the log-likelihood of the model from -5.9 to -4.4 . The final

submodels of each class provide the best segmentation thresholds $t_1 = 64$ and $t_2 = 187$.

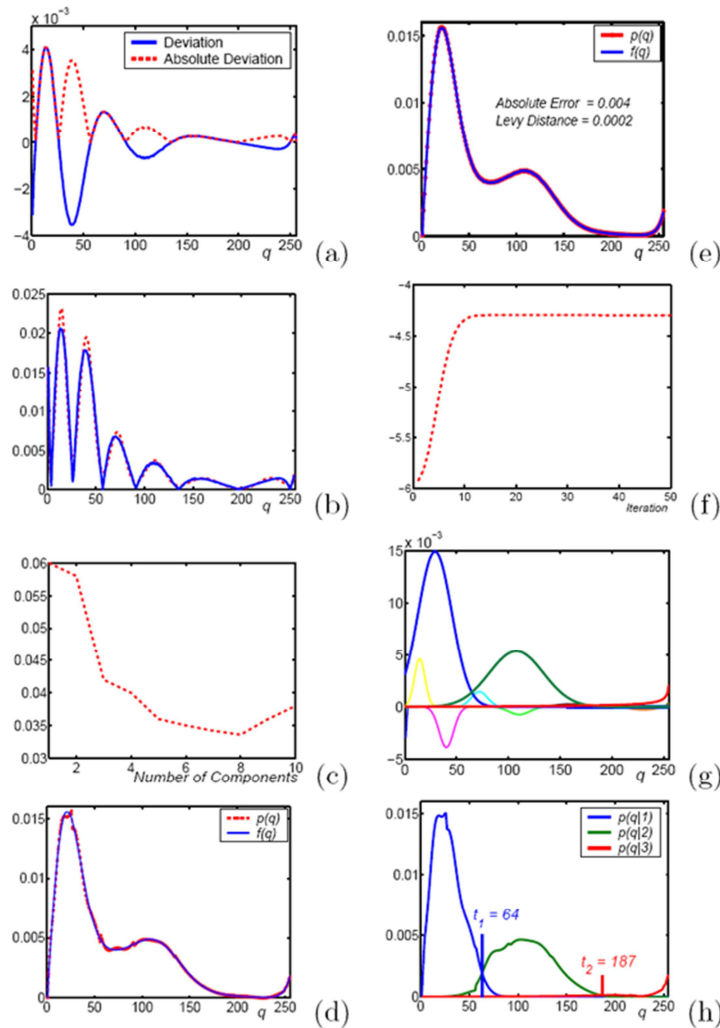


Figure 4: Deviations and absolute deviations $f_{emp}(q) - p_3(q)$ (a), the best mixture (b) to model the absolute deviations, the residual absolute error (c) in function of the number of DGs approximating the deviations, the initial (d) and final (e) 3-class model w.r.t. the empirical distribution, the log-likelihood dynamics (f) for the model refinement, the individual components (g), and the class submodels (h) for the refined model.

Probabilistic Modeling of Blood Vessels for Segmenting Magnetic Resonance Angiography Images

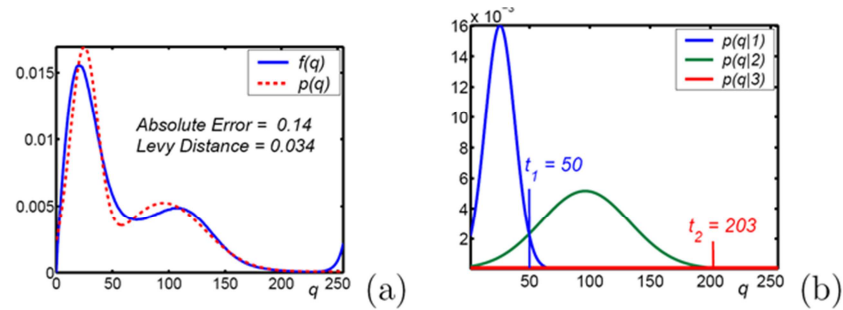


Figure 5: Estimated Wilson-Noble's model [21] (a) and its class submodels (b).

To highlight the advantages of our approach, Fig. 5 shows results obtained with the model of Wilson and Noble [21] (the mixture of two Gaussians and $\varphi_{\text{lam}}(q)$). The quality is evaluated by the Levy distance [36] and the absolute error between the empirical distribution and the estimated 3-class model. In this example, the Wilson-Noble's and our approach result in the Levy distance of 0.14 and 0.0002 and the absolute error of 0.14 and

0.004, respectively. The lower Levy distance and absolute error suggest our approach yields the notably better approximation ensuring more accurate separation of the blood vessels from their background. As shown later in Fig. 8 the typically higher separation threshold of the Wilson-Noble's approach, e.g. $t_2 = 203$ versus our $t_2 = 187$ in this particular example, results in many missed blood vessels.

Probabilistic Modeling of Blood Vessels for Segmenting Magnetic Resonance Angiography Images

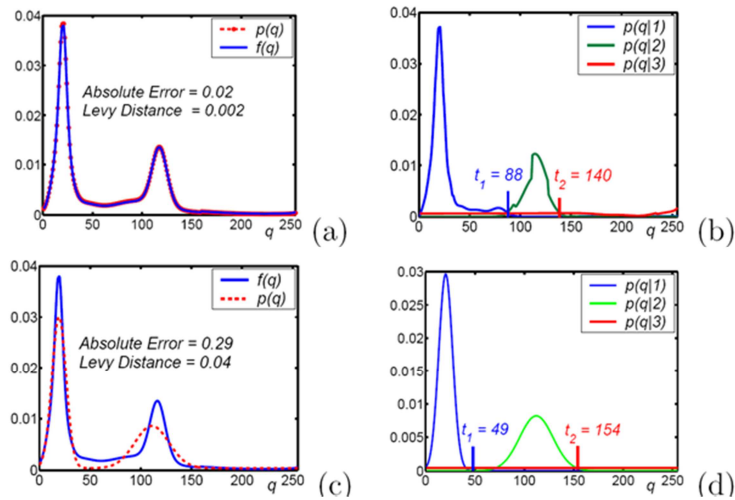


Figure 6: Slice in Fig. 3,B: our final (a,b) and the Wilson-Noble's (c,d) 3-class model (a,c) with the individual class submodels (b,d).

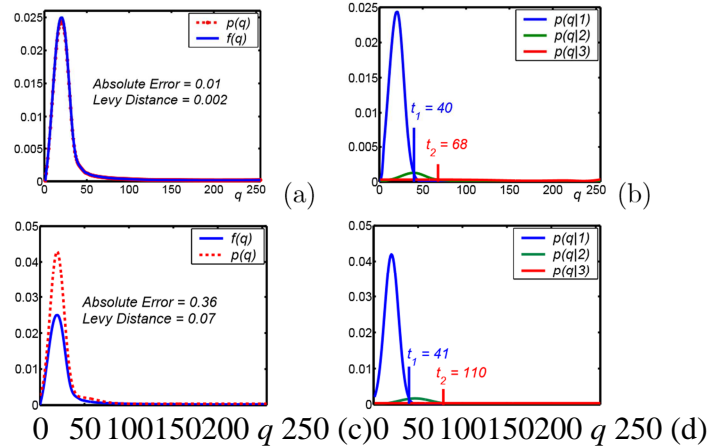


Figure 7: Slice in Fig. 3,C: our final (a,b) and the Wilson-Noble's (c,d) 3-class model (a,c) with the individual class submodels (b,d).

Figures 6 and 7 show our and Wilson-Noble's models estimated for the slices in Figs. 3, B and C, respectively. In these examples our models are more accurate. We compared both the approaches on 50 real MRA data sets, too. Results of the six tests in Fig. 8 as well as

other tests confirm that the Wilson-Noble's approach fails to detect large fractions of vascular trees validated by an expert-radiologist. Our approach is more accurate in restoring detail of the brain vascular tree.

Probabilistic Modeling of Blood Vessels for Segmenting Magnetic Resonance Angiography Images

Table 1: Minimum ε_n , maximum ε_x , and mean ε^- segmentation errors, and standard deviations σ of errors on the geometrical 3D TOF-MRA phantoms for our (OA) and the Wilson–Noble’s (WN) approaches as well as for

three other segmentation algorithms using iterative thresholding (IT) [27] and gradient based (DMG) [18] or gradient vector flow based (GVF) [19] deformable models.

	OA	WN	IT	DMG	GVF
$\varepsilon_n, \%$	0.09	0.10	4.81	10.1	2.45
$\varepsilon_x, \%$	2.10	12.1	33.1	21.8	13.6
$\varepsilon^-, \%$	0.61	6.20	18.8	11.9	5.96
$\sigma, \%$	0.93	7.40	8.41	3.79	2.79

Probabilistic Modeling of Blood Vessels for Segmenting Magnetic Resonance Angiography Images












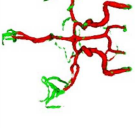





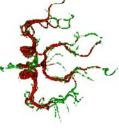
	$t_2 = 119, \beta = 0.05$		$t_2 = 129$	
	$t_2 = 117, \beta = 0.08$		$t_2 = 151$	
	$t_2 = 125, \beta = 0.12$		$t_2 = 180$	
	$t_2 = 68, \beta = 0.038$		$t_2 = 110$	
	$t_2 = 140, \beta = 0.18$		$t_2 = 154$	
	$t_2 = 187, \beta = 0.92$		$t_2 = 203$	
(a)		(b)		(c)

Figure 8: Each row relates to one patient: our (a) and the Wilson-Noble's (b) segmentation, and their differences (c): the red voxels are detected by the both approaches and the green ones are missed by the latter one.

Probabilistic Modeling of Blood Vessels for Segmenting Magnetic Resonance Angiography Images

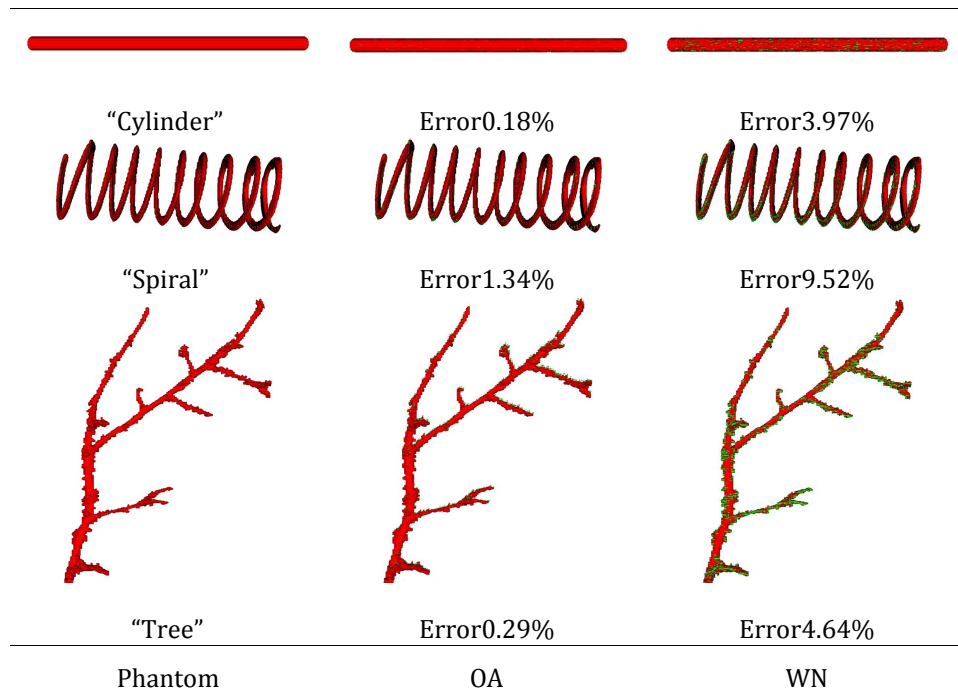


Figure 9: Segmentation of 3D phantoms with our (OA) and the Wilson-Noble's (WN) approaches (the same color code as in Fig. 8).

4. Validation

It is very difficult to accurately get manually segmented **complete** vasculare trees to validate our algorithm. To quantitatively evaluate its performance, we created three 3D phantoms in Fig. 9 with geometrical shapes similar to blood vessels with known ground truth. These three phantoms mimic bifurcations, zero and high curvature existing in any vascular system, and their changing radii simulate both large and small blood vessels. To make the distributions of these three phantoms similar to

MRA images, first we compute the empirical class distributions $p(q|bv)$, $p(q|csf)$, and $p(q|bt)$ from the signals that represent blood vessels, CSF, and brain tissues from the MRA images segmented by a radiologist (we have selected 200 images from a data set of over 5000 images of 50 subjects). Then, The phantoms signal are generated by using the inverse mapping methods. The resulting phantom's histograms are similar to those in Fig. 4(e).

The total segmentation error is evaluated by a percentage of erroneous voxels with respect to

Probabilistic Modeling of Blood Vessels for Segmenting Magnetic Resonance Angiography Images

the overall number of voxels in the ground truth 3D phantom. Figure 9 shows that, on average, our approach is 14 times more accurate than the Wilson-Noble's one. Table 1 gives error statistics for 440 synthetic slices segmented in the phantoms with both approaches and compares them to three other known segmentation algorithms.

Therefore, comparing to the more conventional probability model in [21], our adaptive model notably improves the accuracy of segmenting the MRA images acquired with different scanners. The conventional approaches either assume a purely laminar blood flow or pre-select a simple parametric distribution in attempts to take account of actual signal features. By contrast, our model is derived from the physical description of the blood flow and thus can accurately handle both normal and abnormal cases. Moreover, the estimated weights $\beta \in [0,1]$ in Eq. (1) provide a natural measure of the percentage of abnormality of the blood flow for a particular subject.

References

- [1] A. Chung, J. A. Noble, P. Summers, "Fusing speed

5. Conclusions

We presented a new physically justified adaptive probability model of blood vessels on magnetic resonance angiography (MRA) images. It accounts for laminar (normal subjects) and turbulent blood flow (abnormal cases like anemia or stenosis). Better accuracy of segmenting MRA images with our approach compared to more conventional algorithms is confirmed by experts-radiologists and also validated using special 3D geometrical phantoms.

Our present C++ implementation of the algorithm on a single 2.4 GHz Pentium 4 CPU with 512 MB RAM takes about 49 *sec* to segment 93 TOFMRA slices of size 512×512 pixels each.

The proposed model is suitable for segmenting both TOF-MRA and PCMRA images. Experiments with the latter type was not included in this paper due to space limitations. But the algorithm's code, sample data, and segmentation results for all the MRA images will be provided in our web page.

and phase information for vascular segmentation of

Probabilistic Modeling of Blood Vessels for Segmenting Magnetic Resonance Angiography Images

- phase contrast MR angiograms,” *Medical Image Analysis*, vol. 6, pp. 109–128, 2002.
- [2] C. G. Caro et al., *The Mechanics of the Circulation*, Oxford University Press, 1978.
- [3] W. F. Ganong, *Review of medical physiology*, McGraw-Hill, 15th edition, 1991.
- [4] Y. Sato, S. Nakajimaa, N. Shiragaa, H. Atsumia, S. Yoshidab, T. Kollercc, G. Gerigc, and R. Kikinisa, “Three-dimensional multi-scale line filter for segmentation and visualization of curvilinear structures in medical images,” *Med. Image Anal.*, vol. 2, no. 2, pp. 143–168, 1998.
- [5] K. Krissian, G. Malandain, N. Ayache, R. Vaillant, and Y. Troussel, “Model based multiscale detection of 3D vessels,” in *Proc. IEEE Conf. Comput. Vision and Pattern Recognition*, 1998, pp. 722–727.
- [6] F. Catté, P-L. Lions, J.-M. Morel, and T. Coll, “Image selective smoothing and edge detection by nonlinear diffusion,” *SIAM J. Numerical Anal.*, vol. 29, no. 1, pp. 182–193, 1992.
- [7] C. Lacoste, G. Finet, and I. E. Magnin, “Coronary tree extraction from X-ray angiograms using marked point processes,” in *Proc. IEEE Int. Symp. Biomed. Imaging*, 2006, pp. 157–160.
- [8] M. A. Gu’lsu’n and H. Tek, “Robust vessel tree modeling,” in *Proc. Int. Conf. Med. Image Comput. Computer-Assisted Intervention*, 2008, pp. 602–611.
- [9] M. P’echaud, R. Keriven, and G. Peyr’e, “Extraction of tubular structures over an orientation domain,” in *Proc. IEEE Conf. Comput. Vision and Pattern Recognition*, 2009, pp. 336–342.
- [10] H. Li and A. Yezzi, “Vessels as 4-D curves: Global minimal 4-D paths to extract 3-D tabular surfaces and centerlines,” *IEEE Trans. Med. Imag.*, vol. 26, no. 9, pp. 1213–1223, 2007.
- [11] N. Zhu and A. C. Chung, “Minimum average-cost path for real time 3D coronary artery segmentation of ct images,” in *Proc. Int. Conf. Med. Image Comput. Computer-*

Probabilistic Modeling of Blood Vessels for Segmenting Magnetic Resonance Angiography Images

- Assisted Intervention*, 2011, pp. 436–444.
- [12] A. C. Jalba, M. H. Wilkinson, J. B. Roerdink, “CPM: A deformable model for shape recovery and segmentation based on charged particles,” *IEEE Trans. Pattern Analysis and Machine Intell.*, vol. 26, pp. 1320–1335, 2004.
- [13] L. M. Lorigo, O. D. Faugeras, W. E. Grimson, R. Keriven, R. Kikinis, A. Nabavi, and C. F. Westin, “Curves: Curve evolution for vessel segmentation,” *Med. Image Anal.*, vol. 5, no. 3, pp. 195–206, 2001.
- [14] T. Deschamps and L. D. Cohen, “Fast extraction of tubular and tree 3D surfaces with front propagation methods,” in *Proc. IEEE Int. Conf. Pattern recognition*, 2002, pp. 731–734.
- [15] M. Holtzman-Gazit, R. Kimmel, N. Peled, and D. Goldsher, “Segmentation of thin structures in volumetric medial images,” *IEEE Trans. Image Process.*, vol. 15, no. 3, pp. 354–363, 2006.
- [16] R. Manniesing, B. K. Velthuis, M. S. van Leeuwen, I. C. van der Schaaf, P. J. van Laar, and W. J. Niessen, “Level set based cerebral vasculature segmentation and diameter quantification in CT angiography,” *Med. Image Anal.*, vol. 10, no. 2, pp. 200–214, 2006.
- [17] N. D. Forkert, D. Saring, T. Illies, J. Fiehler, J. Ehrhardt, H. Handels, and A. Schmidt-Richberg, “Direction-dependent level set segmentation of cerebrovascular structures,” in *Proc. SPIE’11, Image Processing: Medical Imaging*, 2011, vol. 7962, pp. 1–8.
- [18] M. Kass, A. Witkin, and D. Terzopoulos, “Snakes: Active contour models,” *Int. J. Comput. Vision*, vol. 1, pp. 321–331, 1988.
- [19] C. Xu and J. L. Prince, “Snakes, shapes, and gradient vector flow,” *IEEE Trans. Image Process.*, vol. 7, no. 3, pp. 359–369, 1998.
- [20] V. Caselles, R. Kimmel, and G. Sapiro, “Geodesic active contours,” *Int. J. Comput. Vision*, vol. 22, no. 1, pp. 61–79, 1997.
- [21] D. L. Wilson and J. A. Noble, “An adaptive segmentation algorithm for time-of-flight MRA data,”

Probabilistic Modeling of Blood Vessels for Segmenting Magnetic Resonance Angiography Images

- IEEE Trans. Med. Imaging*, vol. 18, no. 10, pp. 938–945, 1999.
- [22] A. C. S. Chung and J. A. Noble, “Statistical 3D vessel segmentation using a Rician distribution,” in *Proc. Int. Conf. Med. Image Comput. Computer-Assisted Intervention*, 1999, pp. 82–89.
- [23] A. Webb, *Statistical Pattern Recognition*, J. Wiley & Sons, New York, 2002.
- [24] D. Nain, A. Yezzi, and G. Turk, “Vessels segmentation using a shape driven flow,” in *Proc. Int. Conf. Med. Image Comput. Computer-Assisted Intervention*, 2004, pp. 51–59.
- [25] M. W. Law and A. C. Chung, “A deformable surface model for vascular segmentation,” in *Proc. Int. Conf. Med. Image Comput. Computer-Assisted Intervention*, 2009, pp. 59–67.
- [26] R. Gan, A. C. Chung, C. K. Wong, and S. C. Yu, “Vascular segmentation in threedimensional rotational angiography based on maximum intensity projections,” in *Proc. IEEE Int. Symp. Biomed. Imaging*, 2004, pp. 133–136.
- [27] S. Hu and E. A. Hoffman, “Automatic lung segmentation for accurate quantization of volumetric X-ray CT images,” *IEEE Trans. Med. Imag.*, vol. 20, no. 6, pp. 490–498, 2001.
- [28] J. Mille, R. Bon`e, and L. D. Cohen, “Region-based 2D deformable generalized cylinder for narrow structures segmentation,” in *Proc. Eur. Conf. Comput. Vision*, 2008, pp. 392–404.
- [29] J. Tyrrell, E. di Tomaso, D. Fuja, R. Tong, K. Kozak, R. K. Jain, and B. Roysam, “Robust 3-D modeling of vascuature imagery using superellipsoids,” *IEEE Trans. Med. Imaging*, vo. 26, no. 2, pp. 223–237, 2007.
- [30] T. Chen and D. N. Metaxas, “Gibbs prior models, marching cubes, and deformable models: A hybrid framework for 3D medical image segmentation,” in *Proc. Int. Conf. Med. Image Comput. Computer-Assisted Intervention*, 2003, pp. 703–710.

Probabilistic Modeling of Blood Vessels for Segmenting Magnetic Resonance Angiography Images

- [31] Y. Shang, R. Deklerck, E. Nyssen, A. Markova, J. de Mey, X. Yang, and K. Sun, "Vascular active contour for vessel tree segmentation," *IEEE Trans. Biomed. Eng.*, vol. 58, no. 4, pp. 1023–1032, 2011.
- [32] X. Gao, Y. Uchiyama, X. Zhou, T. Hara, T. Asano, and H. Fujita, "A fast and fully automatic method for cerebrovascular segmentation on time-of-flight (TOF) MRA image," *J. Digital Imaging*, vol. 24, no. 4, pp. 609–625, 2011.
- [33] A. Dufour, N. Passat, B. Naegel, and J. Baruthio, "Interactive 3D brain vessel segmentation from an example," in *Proc. IEEE Int. Symp. Biomed. Imaging*, 2011, pp. 1121–1124.
- [34] W. Liao, K. Rohr, C.-K. Kang, Z.-H. Cho, and S. Wörz, "A generative MRF approach for automatic 3D segmentation of cerebral vasculature from 7 Tesla MRA images," in *Proc. IEEE Int. Symp. Biomed. Imaging*, 2011, pp. 2041–2044.
- [35] M. Sabry, C. B. Sites, A. A. Farag, S. Hushek, and T. Moriarty, "A fast automatic method for 3D volume segmentation of the human cerebrovascular," in *Proc. Computer-Assisted radiology and surgery*, 2002, pp. 382–387.
- [36] G. Gimelfarb, A. A. Farag, and A. El-Baz, "Expectation maximization for a linear combination of Gaussians," in *Proc. IEEE Int. Conf. Pattern Recognit*, 2004, vol. 3, pp. 422–425.
- [37] A. El-Baz, G. Gimelfarb, R. Falk, M. Abou El-Ghar, V. Kumar, and D. Heredia, "A Novel 3D Joint Markov-Gibbs Model for Extracting Blood Vessels from PC-MRA," *Proc. of International Conference on Medical Image Computing and Computer-Assisted Intervention (MICCAI'09)*, London, UK, September 20 - 24, 2009, pp. 943–950.
- [38] A. El-Baz, A. Farag, G. Gimelfarb, M. Abou El-Ghar, and T. Eldiasty, "Probabilistic Modeling of Blood Vessels for Segmenting MRA Images," *Proc. of International Conference on Pattern Recognition (ICPR 06)*, Hong Kong, August 2004, 2006, vol. 3, pp. 917–920.
- [39] A. El-Baz, A. Farag, G. Gimelfarb, M. Abou El-Ghar, and T. El-Diasty, "A

Probabilistic Modeling of Blood Vessels for Segmenting Magnetic Resonance Angiography Images

- New Adaptive Probabilistic Model of Blood Vessels for Segmenting MRA Images,“ Proc. of International Conference on Medical Image Computing and Computer-Assisted Intervention, (MICCAI’06), Copenhagen, Denmark, October 16, 2006, vol. 2, pp. 799-806.
- [40] A. El-Baz, A. Farag, and G. Gimelfarb, “Cerebrovascular Segmentation by Accurate Probabilistic Modeling of TOF-MRA Images,“ Proc. of Fourteenth Scandinavian Conference on Image Analysis (SCIA’05), Joensuu, Finland, June 19-22, 2005, pp. 1128-1137.
- [41] A. El-Baz, A. Farag, G. Gimelfarb, and S. Hushek, “Automatic Cerebrovascular Segmentation by Accurate Probabilistic Modeling of TOF-MRA Images,“ Proc. of International Conference on Medical Image Computing and Computer-Assisted Intervention (MICCAI’05), Palm Springs, California, USA, October 26-29, 2005, vol. 1, pp. 34-42.
- [42] A. El-Baz, G. Gimelfarb, and J. Suri, Editors, “Stochastic Modeling for Medical Image Analysis“, Taylor and Francis, ISBN 9781466599079, January 2016.
- [43] A. El-Baz, “Novel Stochastic Models for Medical Image Analysis.“, PhD thesis, 2006
- [44] A. Farag, A. El-Baz, and G. Gimelfarb, “Precise Segmentation of Multi-Modal Images,“ IEEE Transactions on Image Processing, vol. 15, no. 4, pp. 952-968, April 2006.
- [45] A. El-Baz, A. Farag, and G. Gimelfarb, “Iterative Approximation of Empirical Grey Level Distributions for Precise Segmentation of Multi-Modal Images,“ EURASIP Journal on Advances in Signal Processing, vol. 13, pp. 1969-1983, 2005.